On the effect of pressure coefficient source on the energy demand of an isolated cross-ventilated building

Building and Environment 255 (2024) 111436

Contents lists available at ScienceDirect

Building and Environment

journal homepage: www.elsevier.com/locate/buildenv

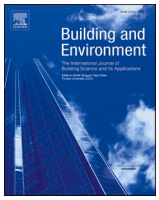

On the effect of pressure coefficient source on the energy demand of an isolated cross-ventilated building

R. Vasaturo [a,*], T. van Hooff [a], S. Gillmeier [a], B. Blocken [b,c], P.J.V. van Wesemael [d]

[a] Building Physics and Services, Department of the Built Environment, Eindhoven University of Technology, Eindhoven, the Netherlands
[b] Institute of Mechanical, Process and Energy Engineering, School of Engineering and Physical Sciences, Heriot-Watt University, Edinburgh, Scotland, United Kingdom
[c] Building Physics and Sustainable Design, Department of Civil Engineering, KU Leuven, Leuven, Belgium
[d] Architectural Urban Design and Engineering, Department of the Built Environment, Eindhoven University of Technology, Eindhoven, the Netherlands

ARTICLE INFO

Keywords:
Large eddy simulation
Natural ventilation
Building energy simulation
Wind pressure

ABSTRACT

Natural ventilation is a simple and effective measure to both reduce the cooling demand of buildings and improve the indoor air quality. In the prediction of heating and cooling demands by means of building energy simulations (BES), the use of pressure coefficients (C_p) from databases as input for the airflow network model is the common approach. C_p values for the same building typology may differ according to the adopted database and are generally unavailable for buildings with complex geometry. Employed C_p values may lead to differences in BES results. This manuscript presents a comparison, for different wind directions, between the C_p distributions and mean values on the facades of a detached building obtained with full-scale CFD – Reynolds-averaged Navier-Stokes (RANS) and large eddy simulation (LES) – simulations, from a database and from wind-tunnel experiments. The obtained pressure coefficients are used in the BES of a naturally ventilated building and the energy demand difference between the four approaches is quantified. Four climate zones (tropical, dry/desertic, temperate, continental) are considered. Although, in terms of accuracy of C_p prediction, LES outperforms RANS for all the wind directions considered, annual cooling energy demand is found to be relatively insensitive to the source of C_p for the current case study, while predicted peak cooling values differ up to 10.8%. On the other hand, the prediction of annual heating energy demand in cold climates varies up to 3% depending on the C_p source employed for BES simulations.

1. Introduction

Natural ventilation can be an effective, cheap and simple method to reduce the cooling demand and the indoor air temperature, and to increase thermal comfort and the indoor air quality of the indoor environment [1]. A substantial reduction of cooling demand and overheating hours can be achieved when this measure is applied. The effects of natural ventilation on the energy demand of several building typologies have been assessed by a variety of studies employing building energy simulation (BES), for instance Pino et al. [2], Ramponi et al. [3], Wang and Chen [4], van Hooff et al. [5,6], Pierangioli et al. [7], and Vasaturo et al. [8], and computational fluid dynamics (CFD). For example, Cheng et al. [9] used CFD to build a methodology for the estimation of natural ventilation coefficients and natural ventilation potential of single- and cross-ventilated flat-roofed buildings. In BES, the effect of natural ventilation can be assessed using airflow network (AFN) models. These models divide internal spaces into single zones (nodes), for which pressure, airflow, temperature and humidity are calculated. In EnergyPlus [10], a validated [11] AFN model is present based on the work of Walton [12]. This model uses the wind pressure coefficients on the building facades as input. The pressure coefficients (C_p) can be obtained from either primary or secondary sources. Cóstola et al. [13] defined full-scale measurements (e.g., Ref. [14,15]), wind-tunnel scale measurements (e.g., Ref. [14,16,17]) and CFD (e.g., Ref. [18–20]) as *primary sources,* and databases [21,22] and analytical models (e.g., Ref. [23–25]) as *secondary sources*. Databases are compilations of pressure coefficients collected from a single or multiple sources [13]. In particular, the database published by Liddament [21] includes, among the others, data for low-rise buildings with two length-to-width ratio (1:1 and 2:1), in sheltered and unsheltered conditions, based on the compilation of the wind-tunnel data reported in the Air Infiltration and Ventilation Centre proceedings [26].

* Corresponding author.
E-mail address: r.vasaturo@tue.nl (R. Vasaturo).

https://doi.org/10.1016/j.buildenv.2024.111436
Received 3 August 2023; Received in revised form 13 March 2024; Accepted 17 March 2024
Available online 19 March 2024

According to de Wit [27,28], the input of C_p is one of the principal causes of uncertainty in BES calculations with AFN, thus affecting the computed energy consumption and thermal comfort. Although wind-tunnel data are the most used primary source of C_p, values of C_p from databases are most widely employed in BES including AFN models [13]; this is a straightforward approach, since no preliminary calculations or experiments have to be performed. As a matter of fact, mean C_p values from databases are given for each building facade depending on certain parameters, such as building geometry and wind direction (e.g. Ref. [21]). However, a limitation of this approach is the unavailability of pressure coefficients for buildings with a more complex geometry, which are generally not present in the database. In addition, different databases may show different C_p values for buildings with the same geometry and configuration [13]. Such limitations are applicable to the Heijmans ONE building [29], which was investigated in the previous work of Vasaturo et al. [8], for which C_p values from a database [21] have been used; as a matter of fact, the Heijmans ONE building is characterized by an asymmetrical gable roof. Hence, a possible solution is represented by obtaining C_p values from CFD and subsequently using them as input for the AFN. In the literature, this process is referred to as a coupling between CFD and BES. Tian et al. [30] reviewed and classified the CFD/BES coupling mechanisms: internal coupling, where CFD and BES have a single solver, and external coupling, where CFD and BES solvers remain separate, but the data are exchanged between the two simulations (statically or dynamically). Other reviews of CFD/BES coupling were reported in the literature (e.g., Ref. [31,32]), while a comprehensive review of coupling strategies between urban microclimate and building energy models, including CFD/BES, was performed by Sezer et al. [33]. Chen et al. [34] suggested that the impact from small scale (indoor airflow) to large scale (outdoor airflow) can be neglected if the opening area does not exceed 20% of the facade. This is referred to by the authors as the one-way approach.

Most of the studies reported in the literature focus on the use of CFD/BES coupling for the improved prediction of building performance (e.g., Ref. [35–41]), while others use BES to compare the values of some key ventilation parameters with those obtained employing CFD, when wind-tunnel or full-scale tests cannot be performed. For example, Asfour and Gadia [42] compared their CFD results with the outcomes of an AFN model, in terms of airflow rate, for various building geometries. Zhai et al. [36] reported differences up to 10% in the prediction of heating and cooling demands for an office building, due to the improved prediction of convective heat transfer coefficients. Similarly, Zhai and Chen [43] reported, for an auto-racing facility, a difference in cooling demand of 39% between coupled and uncoupled simulations. Mochida et al. [38] investigated the cooling load of a cross-ventilated building by means of a static one-way coupling between CFD and BES. Cóstola and Alucci [44] and Wang and Wong [45] ran RANS simulations to compute C_p values to be used as an input to the AFN of a building energy simulation. In particular, Cóstola and Alucci [44] found differences in mean and hourly airflow rate up to 120% and 600%, respectively, when employing C_p values from databases or CFD. Wang et al. [46] demonstrated the capabilities of the software CONTAM 3.0, a multizone building airflow and contaminant transport simulation tool, for a low-rise residential building. In particular, C_p values at the building surface, computed using RANS simulations, allow for an improvement in the prediction of air infiltration. Charisi et al. [47] investigated the effect of C_p from different sources, including databases and CFD, on the BES results of a low-rise, pitch-roofed building, and showed that using C_p from CFD led to the most accurate results in terms of infiltration rate. Moreover, several authors (e.g., Ref. [20,48–51]) showed that large eddy simulations (LES) outperform Reynolds-averaged Navier-Stokes (RANS) in the prediction of pressure coefficients on building facades, especially for lateral and leeward facades. On the other hand, for simulations of wind flow around buildings, the computational cost of LES is much higher than RANS (e.g. Ref. [52]).

To the best knowledge of the authors, the problem of the impact of the source of C_p values on the energy consumption of a cross-ventilated building with a complex geometry has only been partially addressed in the literature. In addition, for the considered building typology, no sensitivity analysis involving at the same time pressure coefficients (to be employed in BES) from LES, RANS, wind tunnel experiments and database has been carried out in previous research. In the present manuscript, BES simulations are performed using C_p values from (I) a database [21] of C_p values for an unsheltered, low-rise building, with a length-to-width ratio of 2:1, (II) wind tunnel data, and (III) CFD (both RANS and LES). Thus, a one-way static CFD/BES coupling, according to the classifications of Tian et al. [30] and Chen et al. [34], is adopted. The aim of the work is to assess the effect of the source of C_p values on the heating and cooling demands of the Heijmans ONE building for four different climates (tropical, dry/desertic, temperate, continental). In Section 2 the geometry of the building and the wind-tunnel setup are briefly summarized. Section 3 presents the numerical setup and the results of the CFD simulations in terms of pressure coefficients on the building. In Section 4 the setup and the results of the building energy simulations are presented for the Heijmans ONE building for four different climate zones. Sections 5 and 6 present discussion and conclusions, respectively.

2. Experimental setup

The wind tunnel measurements on the model building are carried out in the Wind Tunnel Laboratory of the Eindhoven University of Technology (TU/e). The test section of the TU/e wind tunnel is 3×2 m^2 (W $\times$ H). This wind tunnel can be used to generate both atmospheric boundary layer (ABL) profiles and uniform flows. The model building is based on the Heijmans ONE building [29], a lightweight semi-portable building commercialized by Heijmans B.V., a construction services company from the Netherlands. The commercial target group of the Heijmans ONE building are young professionals living in peripheral urban areas who rent the house for a competitive price [53]. Main peculiarities of the building are the high energy efficiency, the compactness and, as far as the geometry is concerned, the asymmetrical gable roof (Fig. 1). The model building is made of PMMA with a scale factor of 1:40 with respect to the full-scale building (Figs. 1-2a), resulting in a reduced-scale building height, width and length of 13.75 cm, 7.50 cm and 20.25 cm, respectively.

The neutral ABL velocity profile in the wind tunnel is obtained using both vortex generators and surface roughness elements (Fig. 2). To determine the incident flow characteristics, i.e. the vertical profiles of mean velocity and turbulence intensities in the empty wind tunnel at the location where the building would be positioned [54], streamwise (u), lateral (v) and vertical (w) velocity components are measured using a Series 100 Cobra probe at a sampling frequency of 1000 Hz for a duration of 120 s. The setup, shown in Fig. 2, results in an incident flow profile of mean (time-averaged) streamwise velocity components (U) that can be described by a logarithmic law with a reduced-scale aerodynamic roughness length of $z_0 = 0.01$ m. This roughness length corresponds to a moderately rough terrain roughness classification [55], which is in line with the intended site characteristics of such buildings. The incident mean streamwise refence velocity (U_H) at the building height (H) is 6.86 m/s, and the Reynolds number based on H is 6.2×10^4. The corresponding streamwise turbulence intensity (TI_U) profile is shown in Fig. 2e and can be approximated by the following expression (e.g. Ref. [56])

$$TI_U = ae^{\left(-b\frac{z}{H}\right)} \tag{1}$$

with a = 27.89 and b = 0.1935.

The angles of attack (Fig. 2), α, tested in the wind tunnel are 0°, ±45°, ±90°, ±135°, 180°; in order to test the different wind directions, the building is rotated by means of a turntable. The blockage ratio, defined as the ratio between the frontal area of the building and the

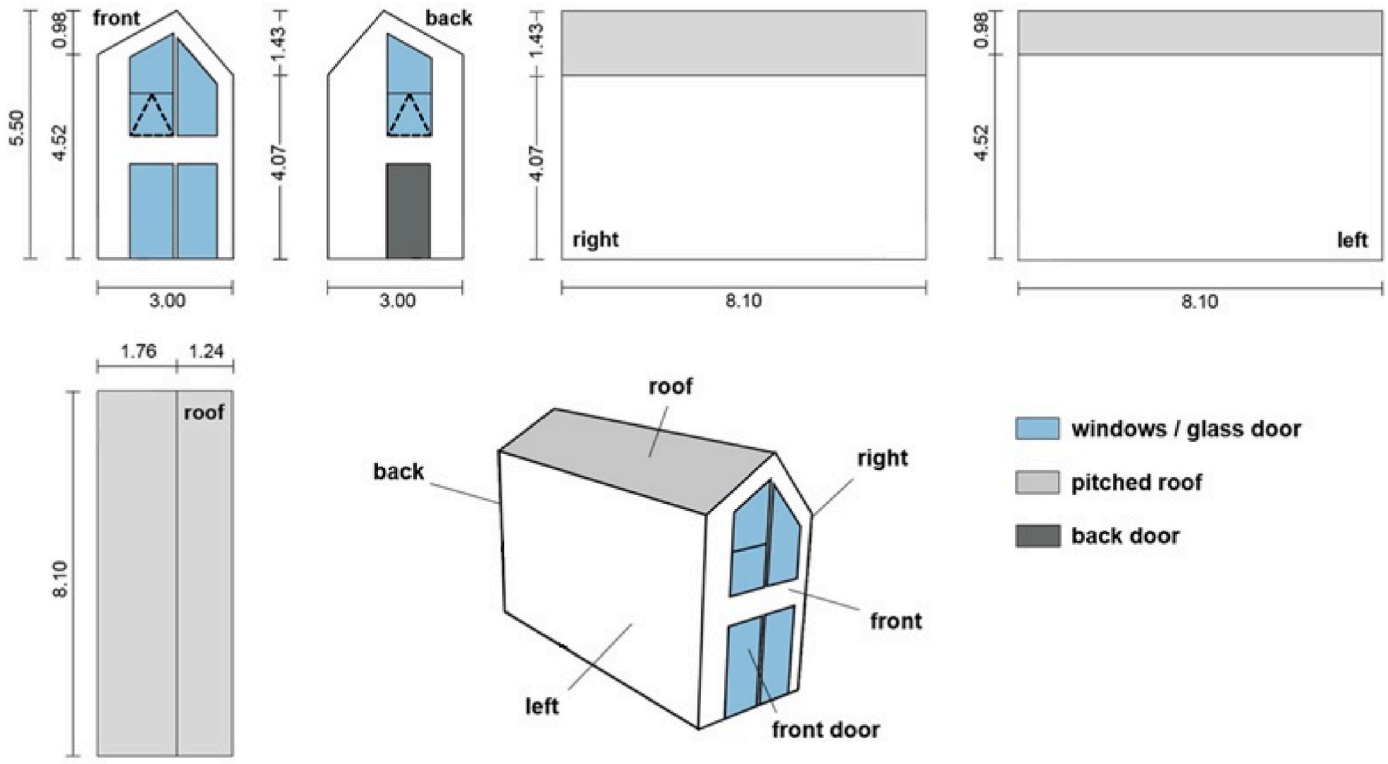

Fig. 1. Full-scale building. Dimensions in m. Dashed triangled windows are openable, with an opening area of 0.9 m^2.

cross-section of the wind tunnel, is well below the recommended threshold of 3% (e.g. Ref. [57]) for all the wind directions considered. Pressure is measured on the model building by means of 128 taps, with a diameter of 1.55 mm each. For this, two Scanivalve MPS4264 pressure scanners with 64 transducers each are employed for simultaneous recording of surface pressures. Data are sampled at 800 Hz for 3 min for each wind direction. The experimental uncertainty (determined by means of repetition measurements) in terms of pressure coefficient is ±0.07.

3. CFD simulations

3.1. Computational domain and grid

The CFD simulations reported in the present manuscript are performed on the full-scale building immersed in a neutral ABL. Hence, the dimensions of the building in the computational domain are the same as reported in Fig. 1. Given the symmetry of the building along a cross-sectional plane parallel to the front and back facades, CFD simulations are performed for only five building orientations (i.e., wind directions) instead of eight. The wind directions are α = 0°, ±45°, ±90° (Fig. 2). The computational domain used for the CFD simulation with zero angle of attack are $L_D \times W_D \times H_D = 16.5H \times 10.4H \times 5H$ in the longitudinal, lateral and vertical direction, respectively (Fig. 3a); there are minor differences in the domain size for different building orientations, as shown in Fig. 3b and c. The distance of the inlet and outlet planes from the building walls is 5H for inlet and lateral boundaries, respectively, in order to comply with the best practice guidelines (e.g., Ref. [57–59]). The adopted distance from the outlet boundary is 10H for all the simulations.

A non-conformal grid is used to discretize the computational domain (Fig. 4). As shown in previous studies (e.g. Ref. [60]), the computational effort can be greatly reduced using this meshing technique without compromising the accuracy of the simulation. In particular, the domain is divided into two subdomains (Ω_1, Ω_2, Fig. 3). A non-orthogonal structured grid composed of hexahedral elements is used in the majority of the cases. Nevertheless, given the complex building geometry, an unstructured grid with tetrahedral elements is employed locally in the subdomain Ω_1 for the cases with α = ±45°. For the case with α = 0°, the coarse grid resulted in a total amount of 10.5 million cells (6.1 million in Ω_1, 4.4 million in Ω_2, see Table 1; Fig. 5a). The minimum and maximum cell size employed to discretize the building are 0.01 m and 0.04 m, respectively, while the maximum cell size in the Ω_1 domain is 0.2 m. The average y^+ on the building surface is 119 (for the case with α = 0°).

In addition, a finer grid of 29.1 million cells (Fig. 5b) is adopted in order to assess the grid resolution; in this case, the minimum and maximum cell edges on the building and the maximum cell edge in the Ω_1 domain are halved with respect to the coarse grid. In order to set up the computational domain for different wind directions, the building is rotated and the Ω_1 subdomain is adjusted accordingly (Fig. 3c); this solution is adopted in order to keep the flow at the inlet boundary perpendicular to the boundary itself, since the vortex method is used as inflow generator for LES. As a matter of fact, in ANSYS Fluent [61] the VM does not provide accurate turbulence generation when oblique flow at the inlet is present.

3.2. Boundary conditions

The vertical profile of mean streamwise velocity at the inlet of the computational domain is obtained from fitting the experimental data. Specifically, a logarithmic law is employed

$$U(z) = \frac{u^*_{ABL}}{\kappa} \log\left(\frac{z + z_0}{z_0}\right) \quad (2)$$

In Eq. (2), $\kappa = 0.42$ is the von Kármán constant, $u^*_{ABL} = 0.304$ m/s the ABL friction velocity, $z_0 = 0.01$ m the aerodynamic roughness length and z the vertical coordinate. The reference wind speed of the undisturbed flow is $U_{ref} = 5$ m/s at a reference height of $h_{ref} = 10$ m. Note that

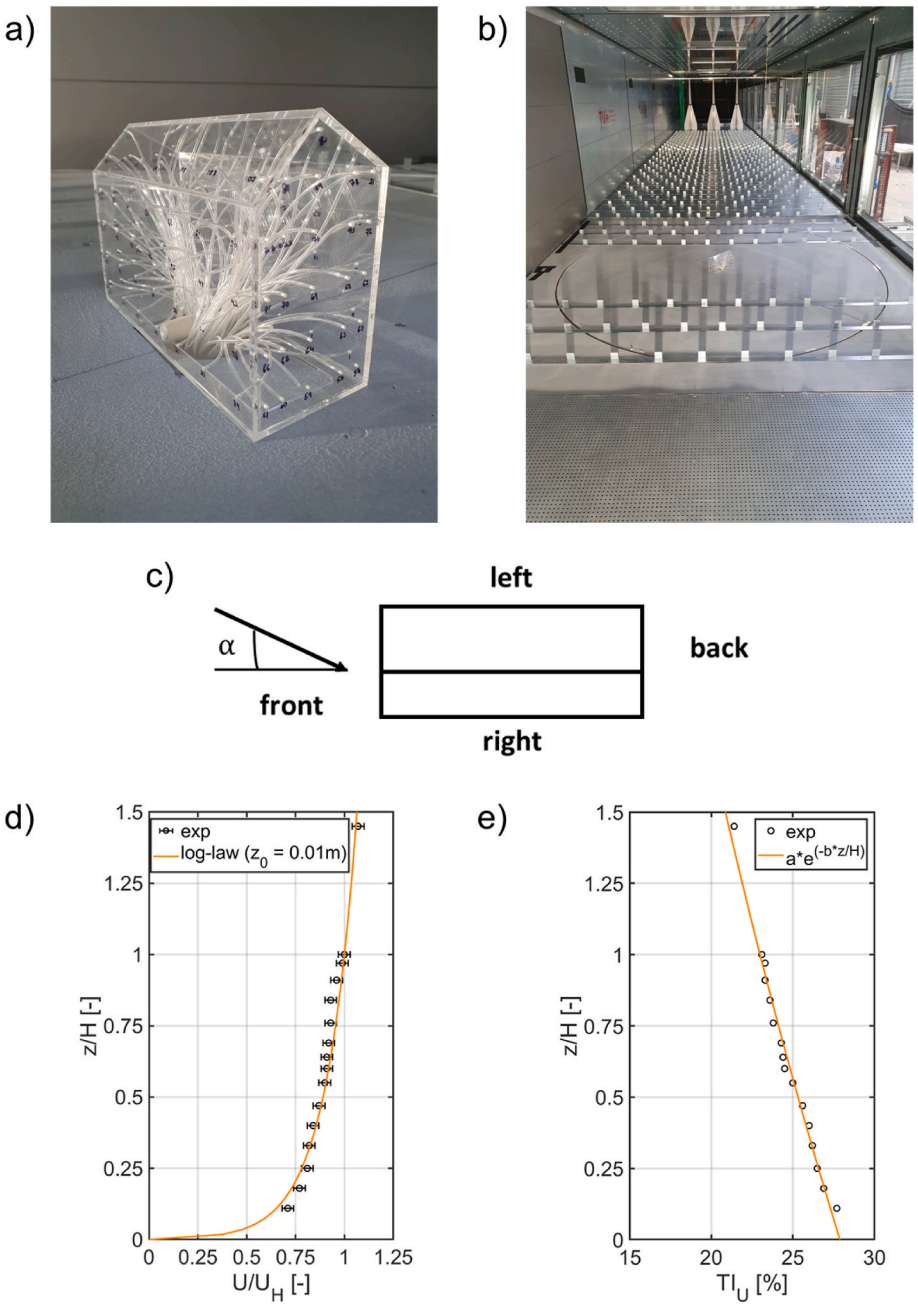

Fig. 2. a) Wind-tunnel scale model building; b) experimental setup (in the wind tunnel test section); c) facade naming and angle of attack conventions for the model building, d) incident mean streamwise velocity profile and fitted logarithmic law; e) incident vertical profile of streamwise turbulence intensity (a = 27.89; b = 0.1935).

although the reference speed and height are different from experimental values, the results are reported in dimensionless form (C_p) and the flow is considered to be Reynolds number independent (e.g. Ref. [62,63]), therefore, they are not affected by the chosen reference values. A zero-shear stress condition is imposed at the lateral and upper boundaries of the domain, whereas at the outlet plane a zero-diffusion flux condition is employed (as in, e.g. Ref. [64]). The wall boundary condition is applied to building walls and ground surface. The commercial software ANSYS Fluent 15 [61] is used to run the CFD simulations. The vortex method [65–67] is used as inflow turbulence generator with a number of vortices of 190 (e.g., Refs. [68–73]). The choice of this method is based on the results shown in previous ABL research [64,74], according to which this method offers the best combination of computational cost and accuracy among the inflow generators implemented in ANSYS Fluent 15. Turbulence kinetic energy and dissipation rate profiles imposed at the inlet for the generation of synthetic turbulence are those reported in Eqs. (3) and (4) [75]:

$$k = \frac{\left(u^*_{ABL}\right)^2}{\sqrt{C_\mu}} \tag{3}$$

$$\varepsilon(z) = \frac{\left(u^*_{ABL}\right)^3}{\kappa(z + z_0)} \tag{4}$$

where C_μ is a model constant equal to 0.09.

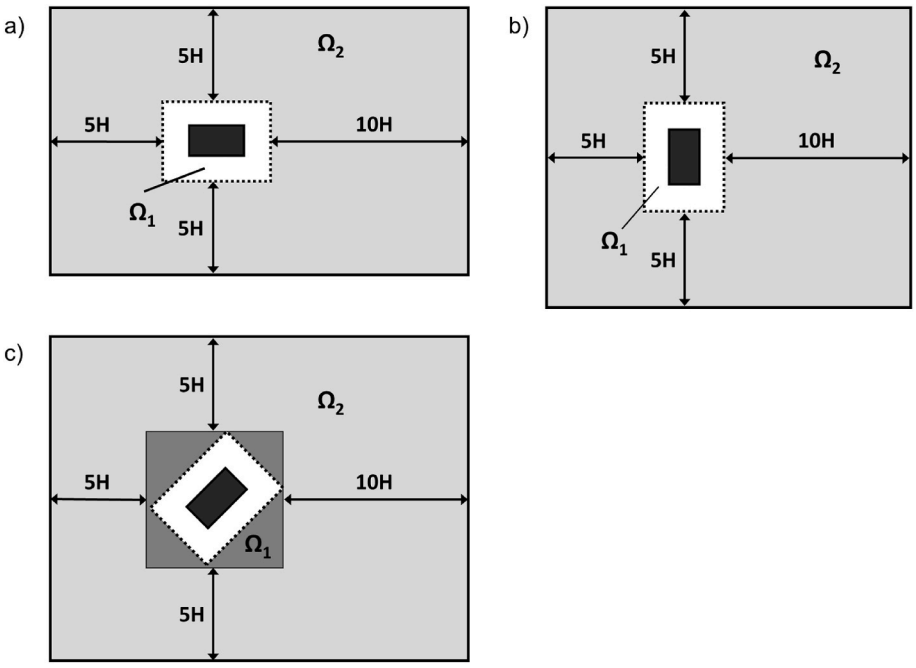

Fig. 3. a) Schematic of the computational domain for 0°, b) ±90° and c) −45° wind directions. Ω_1 and Ω_2 indicate the two subdomains.

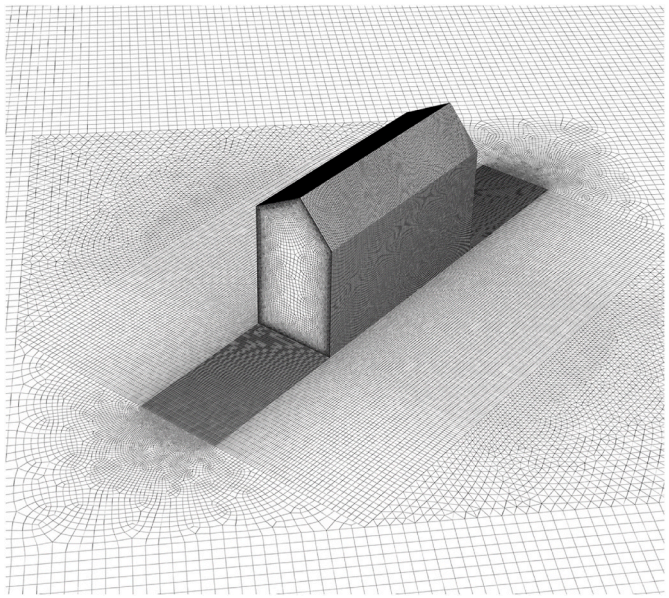

Fig. 4. View of the computational grid (coarse grid; 11.4 million cells) for the model building at −45° wind direction.

Table 1
Number of cells for each subdomain. 0° wind direction.

Subdomain	coarse grid	fine grid
Ω_1	6.1×10^6	18.2×10^6
Ω_2	4.4×10^6	10.9×10^6
total	$\mathbf{10.5 \times 10^6}$	$\mathbf{29.1 \times 10^6}$

3.3. Numerical settings

LES and RANS approaches are used to obtain the flow field. As for LES, the non-iterative time advancement (NITA) scheme is employed to combine both accuracy and computational cost, as reported in the literature (e.g., Refs. [60,64,74,76,77]). The fractional-step scheme is used for pressure-velocity coupling [61,78–82]. In order to prevent unwanted oscillations of the numerical solution, the bounded central differencing scheme is employed for the momentum equation. Finally, second-order schemes are used for pressure interpolation, subgrid kinetic energy and time advancement. A constant time step size is set to obtain a maximum cell convective Courant number lower than 1, i.e., 7.5×10^{-4} s for the simulations with the coarse grid and 5.0×10^{-4} s for the simulation with the fine grid. The kinetic energy transport (KET) subgrid-scale model [83] is used for all simulations. The LES calculations are initialized using the RANS results. The RANS simulations employ second-order schemes and the realizable k-ε [84] turbulence model, with scalable wall functions. To avoid initialization effects, the LES calculations are run for a period of about 5 flow-through times before sampling statistics. The sampling period, sufficient to achieve the statistical convergence of the solution, determined by observing the values of mean pressure and mean velocity at specific points in the domain, corresponds to about 15 domain flow-through times. Both LES and RANS results are eventually compared to the pressure coefficients obtained in the wind tunnel.

3.4. Results

The results are reported along horizontal and vertical lines on the building facades. In particular, horizontal lines are taken at z/H = 0.47; vertical lines are taken in the middle of the right and left facades, while for the front and back facades those lines connect the top vertex to the ground surface. The pressure coefficient, C_p, is defined as follows

$$C_p = \frac{(P - P_{ref})}{0.5\rho U_{ref}^2} \tag{5}$$

where P is the static pressure at a given point on the building, P_{ref} is the reference static pressure and $0.5\rho U_{ref}^2$ is the reference dynamic pressure, taken in the undisturbed flow at the reference height, h_{ref}.

3.4.1. Grid sensitivity study

As previously mentioned, the results of CFD simulations on two different non-conformal grids (coarse and fine) are evaluated in order to

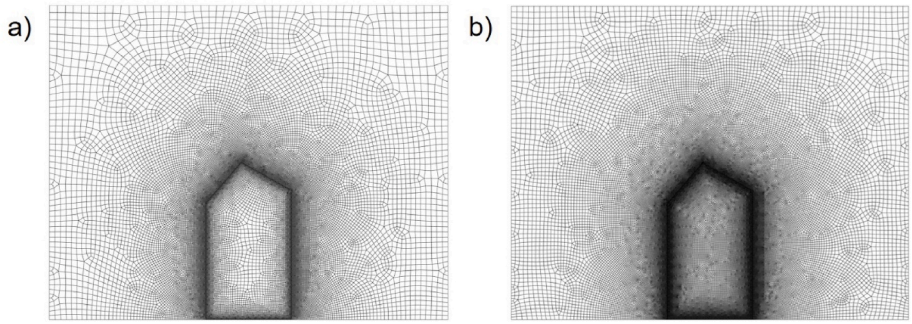

Fig. 5. Lateral cross-section of the computational grid: (a) coarse grid (10.5 million cells); (b) fine grid (29.1 million cells); 0° wind direction.

assess the effect of the grid resolution. The topology of the two grids is reported in Section 3.1. The results are compared along horizontal (Fig. 6) and vertical lines (Fig. 7) in terms of C_p for all the building facades for $\alpha = 0°$. For most of the locations considered the differences are limited, except for some locations at the lateral facades. Quantitatively, along the horizontal lines the mean absolute deviation between coarse and fine grid is 8%, while for the vertical lines it is 11%. It must be noted that for most values considered, the higher deviation in percentage is attributable to the small values of C_P involved. On the other hand, the mean absolute deviation is 0.025 for horizontal lines and 0.033 for vertical lines; these values are below the experimental uncertainty reported in Section 2.

In addition, the LES index of quality (LES IQ) by Celik et al. [85], defined as the ratio between the resolved and the total turbulence kinetic energy (Eq. 6), is evaluated for three lines around the building for the two grids.

$$LES\ IQ = \frac{k_{res}}{k_{tot}} \tag{6}$$

Pope [86] recommended that at least 80% of the turbulence kinetic energy should be resolved, while Celik et al. [85] considered a value of LES IQ of 0.80 ± 0.05 acceptable. The LES IQ is higher or equal to 0.75 for the majority of the locations considered for lines b and c, while lower values are present along line a and, in general, locally (Fig. 8). As a further example, average values of LES IQ in a longitudinal plane crossing the roof ridge, bounded by lines at h/4 from all three sides of the building, are 0.76 for the coarse grid and 0.79 for the fine grid. Furthermore, locally higher percentages of turbulence are resolved by the coarser grid compared to the fine grid; this possibility was reported in other studies and attributed to the effect of the grid resolution on the values of the resolved strain rate tensor [60,85]. Hence, giving the minor differences in terms of both C_p values and LES IQ values, the coarse grid is deemed adequate for the present case and therefore adopted for all the wind directions considered in the present study.

3.4.2. Validation study

LES and RANS results are compared with experimental wind-tunnel data for horizontal (Fig. 9) and vertical lines (Fig. 10) in terms of $C_p$ts for all the building facades (for each wind direction). As well-known and previously reported in literature, it is expected that the C_p provided by LES are more accurate than those obtained using RANS (e.g., Ref. [13,20,48–51]). In order to assess the results, two validation metrics are adopted; the first one is the factor of observation FAC1.3 defined as [87].

$$\mathrm{FAC1.3} = \frac{1}{N}\sum_{i=1}^{N} n_i \quad \text{with} \quad n_i = \begin{cases} 1 \text{ if } & 0.77 \le \dfrac{P_i}{O_i} \le 1.3 \\ 0 & \text{otherwise} \end{cases} \tag{7}$$

P_i and O_i are the predicted and observed data, respectively. On the other hand, the hit rate [87] is used, which is defined as

$$h = \frac{1}{N}\sum_{i=1}^{N} n_i \quad \text{with} \quad n_i = \begin{cases} 1 \text{ for } & \left|\dfrac{P_i - O_i}{O_i}\right| \le D_h \text{ or } |P_i - O_i| \le W_h \\ 0 & \text{otherwise} \end{cases} \tag{8}$$

D_h and W_h are the allowed relative and absolute deviations. In the present study, $D_h = 30\%$ and $W_h = 0.07$, equal to the uncertainty of experimental data. For $\alpha = 0°$ and $\alpha = \pm 90°$, RANS and LES results are comparable for the windward facade; on the other hand, an overestimation of the pressure coefficient is present for all the other facades. Along all the horizontal lines, the hit rate values, calculated for each wind direction, are higher than or equal to 0.88, while the FAC1.3 is higher than 0.70 (Table 2). In particular, for $\alpha = 0°$ an underestimation of the pressure coefficient is observed for the windward facade, and, on the other hand, an overestimation is present for the other facades; however, Fig. 9 shows that for most of the locations considered, the LES results fall within the uncertainty of the experiments (represented by the error bars in the C_p plots). As expected, RANS results differ significantly from the experiments, with both a hit rate and a FAC1.3 equal to 0.21. Similarly, for $\alpha = \pm 45°$, RANS results are closer to the experiments for the two windward facades, while the pressure coefficient is largely

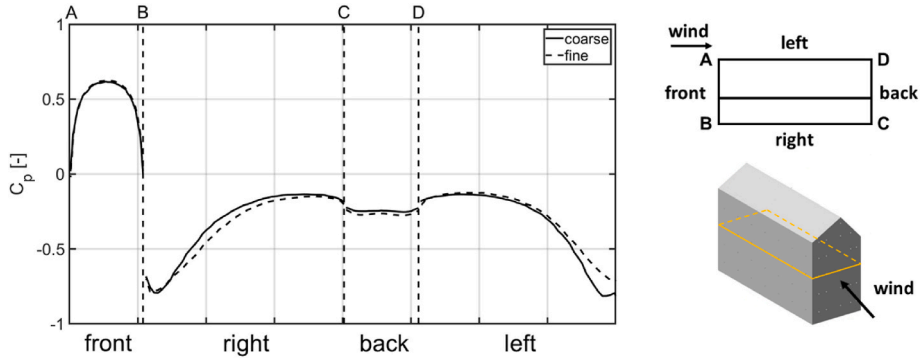

Fig. 6. C_p on the building along horizontal lines (taken at z/H = 0.47) for $\alpha = 0°$. Comparison between coarse and fine grid.

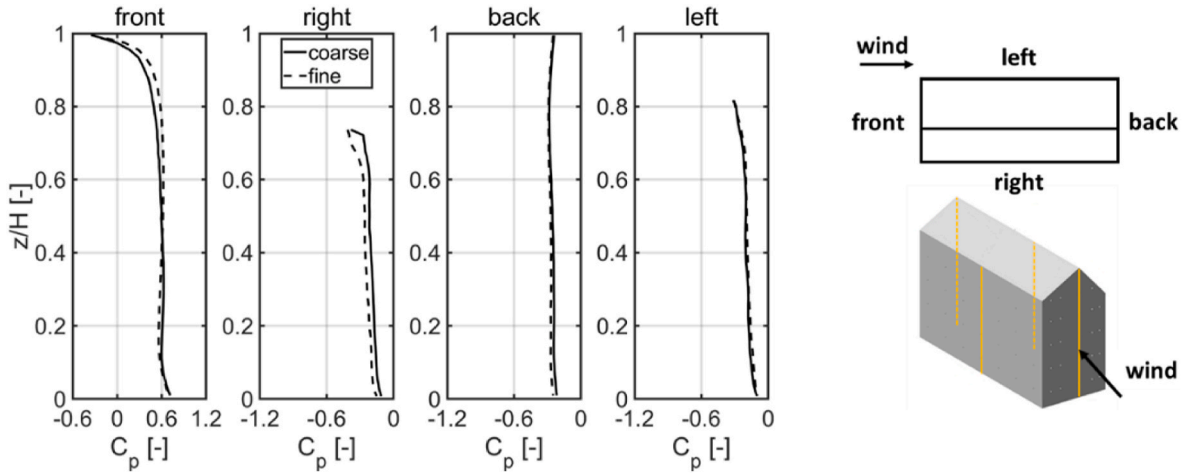

Fig. 7. C_p on the building along vertical lines for $\alpha = 0°$. Comparison between coarse and fine grid.

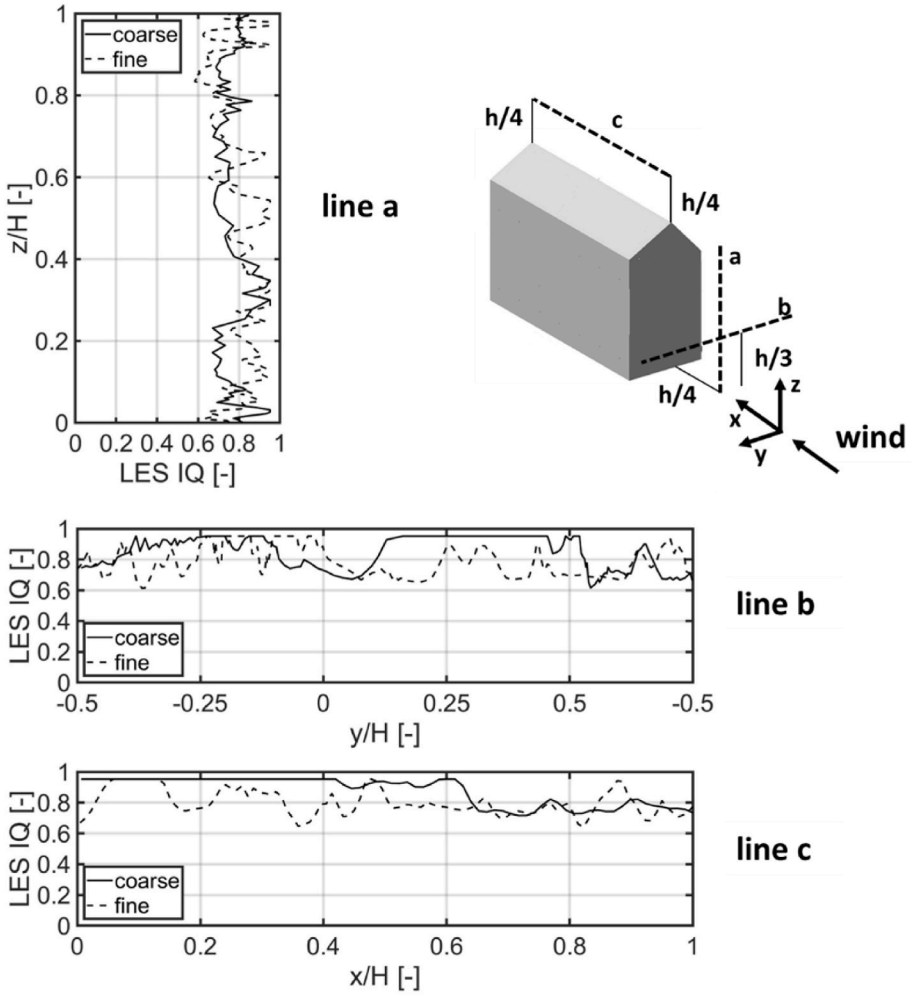

Fig. 8. LES IQ along three lines around the building. Comparison between coarse and fine grid.

overpredicted for leeward facades. The validation metrics are both lower than 0.25, while they are satisfactory for LES ($h = 0.88$, FAC1.3 $\geq$ 0.79 for both wind directions). It is worthwhile to notice that the C_p values near the windward corner (i.e., the corner between the short and long windward facades for oblique wind directions) are erroneously predicted with both numerical techniques. For $\alpha = \pm 90°$, an excellent agreement is found for LES for all the facades, as confirmed by the validation metrics in Table 2. As observed for $\alpha = 0°$ as well, the prediction of C_p obtained using RANS is satisfactory for the windward facade, but not for the lateral and leeward ones (Fig. 9).

The results for the vertical lines are reported in Fig. 10 and Table 3. For the 0° wind direction the most significant difference is observed for

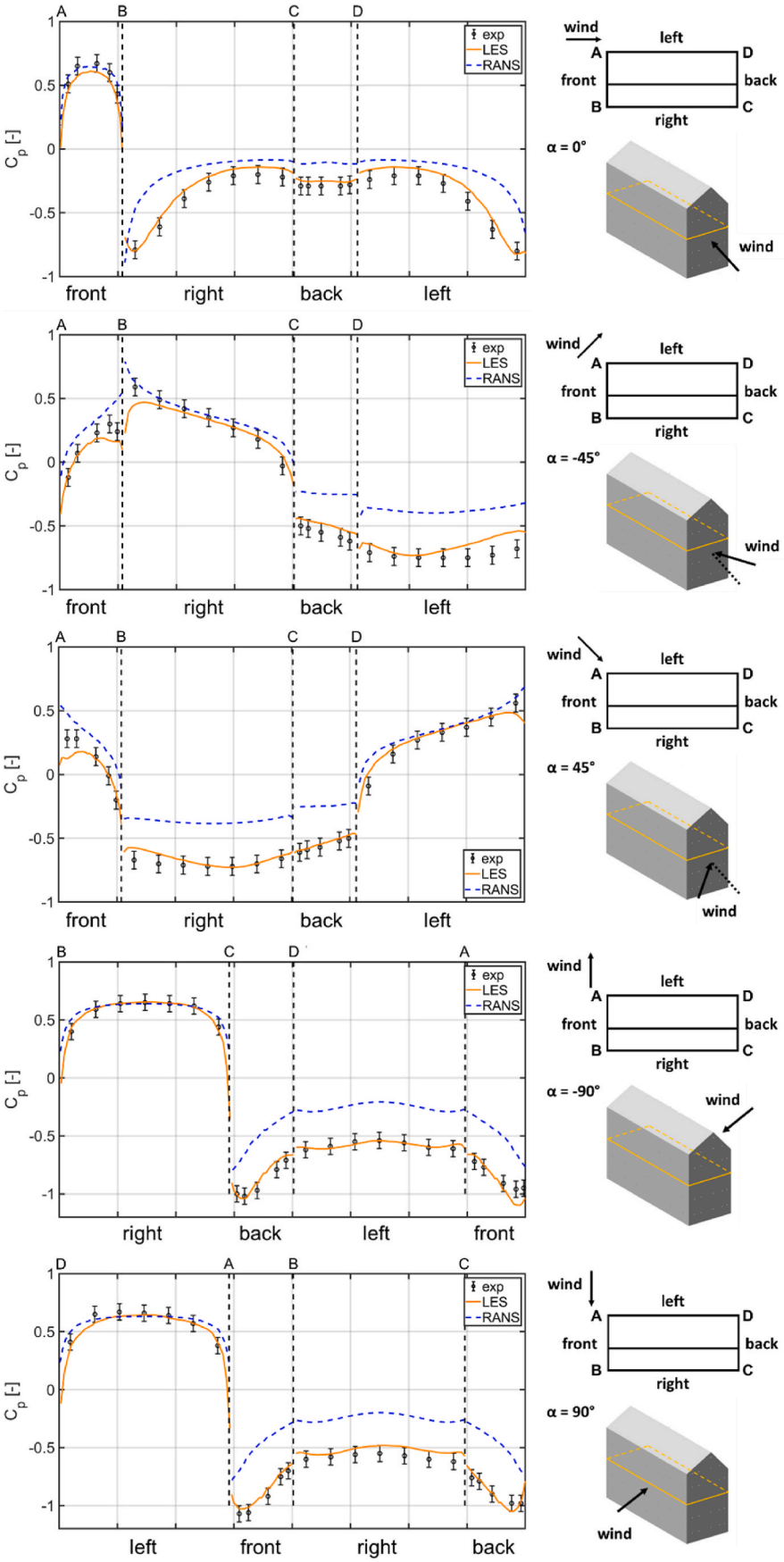

Fig. 9. C_p on the building along horizontal lines for 5 wind directions. Comparison between CFD and experiments.

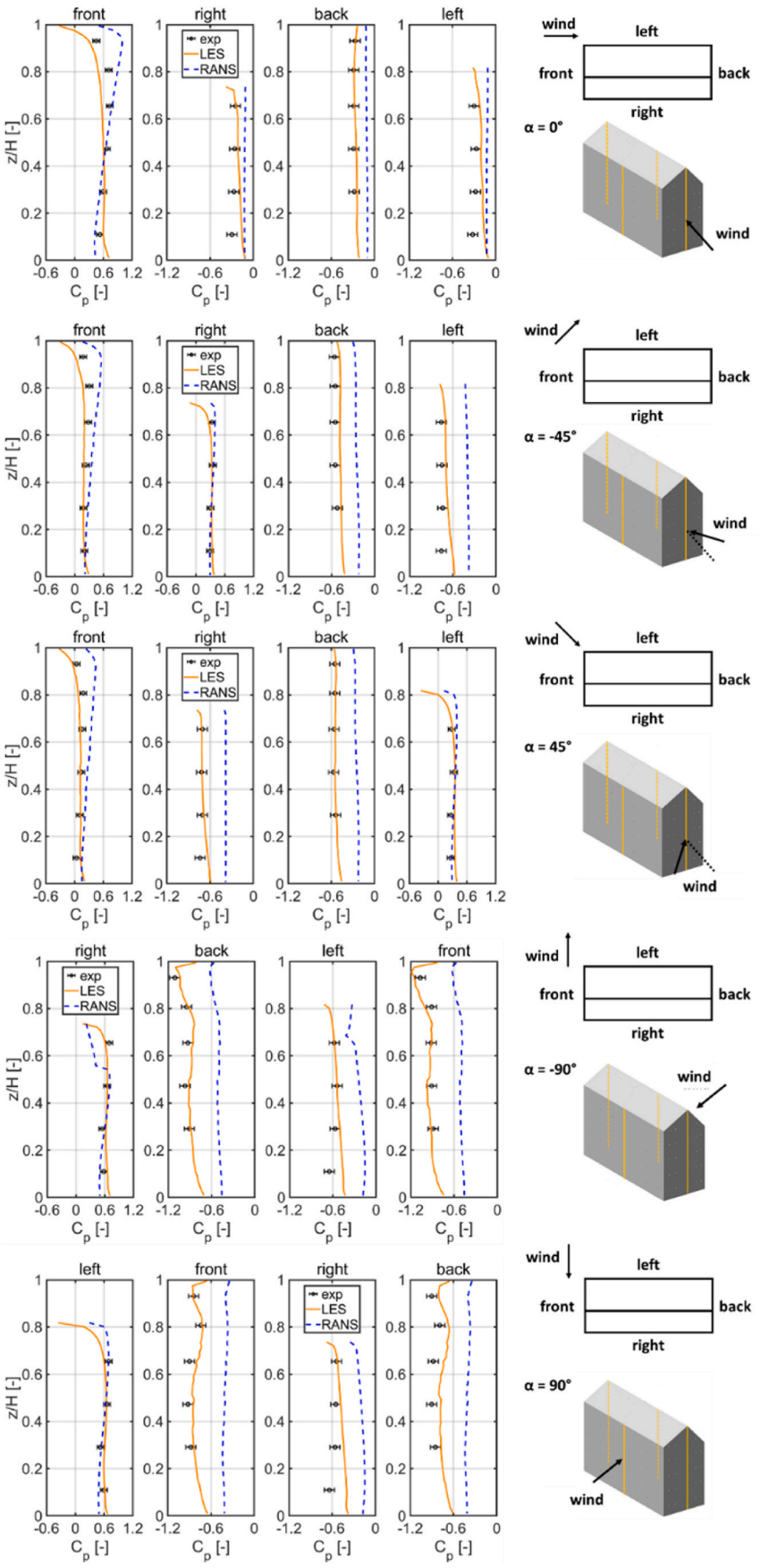

Fig. 10. C_p on the building along vertical lines for 5 wind directions. Comparison between CFD and experiments.

Table 2
Validation metrics for all wind directions. Horizontal lines.

α[°]	Approach	FAC1.3	HR	ideal value
0	RANS	0.21	0.21	1
	LES	0.71	0.96	
−45	RANS	0.25	0.25	1
	LES	0.79	0.88	
45	RANS	0.08	0.12	1
	LES	0.83	0.88	
−90	RANS	0.33	0.37	1
	LES	1	1	
90	RANS	0.25	0.29	1
	LES	1	1	

Table 3
Validation metrics for all wind directions. Vertical lines.

α[°]	Approach	FAC1.3	HR	ideal value
0	RANS	0.26	0.26	1
	LES	0.60	0.74	
−45	RANS	0.26	0.26	1
	LES	0.84	0.84	
45	RANS	0.16	0.16	1
	LES	0.79	0.79	
−90	RANS	0.21	0.21	1
	LES	0.89	0.95	
90	RANS	0.21	0.21	1
	LES	0.89	0.89	

the front facade. As a matter of fact, the experimental data show that the point where the C_p reaches its maximum value is located at z/H ≈ 0.8. CFD simulations predict different results according to the numerical technique employed. For RANS, this point is located above z/H = 0.9. For LES, the predicted C_p values increase towards the bottom, while they are underpredicted in the upper part of the front facade.

In addition, for the 0° case the C_p values are overpredicted for lateral facades, particularly in the lower part of the building (z/H < 0.3), while a satisfactory agreement is obtained for the back facade when LES is used. The hit rate for LES is 0.74, while a FAC1.3 of 0.60 is obtained; those values decrease to 0.26 for RANS. For the α = ±45° cases the underprediction of C_p for the front facade is also displayed by LES. In spite of that, validation metrics show the adequacy of the predicted results with LES; as a matter of fact, the hit rates are 0.88 and 0.79 (Table 3). When RANS is used, a considerable overprediction of C_p is obtained for leeward facades, due to the RANS inaccuracy in simulating flow separation zones and vortex shedding [88]. Finally, for α = ±90° cases, the LES results are generally satisfactory; a general slight overprediction of C_p is present; this prediction becomes significant for the lower part of the leeward facade (*left* for α = −90°, *right* for α = +90°). On the other hand, for these wind directions the RANS results largely overpredict the C_p for most of the facades. Consequently, the values of validation metrics are far from the ideal value when this numerical technique is employed, and CFD simulations cannot be considered as validated.

The area-averaged pressure coefficients from experiments, CFD and databases [21] for the *front* and *back* facades are reported in Figs. 11 and 12. The facade-averaged experimental C_p value is determined by averaging the 25 values corresponding to the measurement locations, while for CFD the values are averaged over the entire facade. These values are relevant since they are used as input for the BES described in Section 4. The facade-averaged C_p values obtained using RANS overpredict the experimental values for all wind directions; a satisfactory agreement is obtained for the *front* facade at α = 0°, while larger differences are found for the other facades, possibly due to the inaccurate prediction of flow separation zones by RANS, as previously reported. In that respect, LES is in closer agreement with experiments than RANS for the *back* facade, and for the *front* facade with α = ±90°, while facade-averaged C_p values are underpredicted for α = 0, ±45°. Both experiments and LES results differ from the C_p values from Liddament [21] by a maximum of 20% for α = 0°; the difference increases above 50% for α = 45°, whereas minor differences are found for ±90° (up to about 3% for experiments and 12% for LES).

Similarly, for the *back* facade the C_p values predicted by LES are in good agreement with experiments, while they are largely overestimated by RANS also for the case of zero angle of attack. For the case with zero angle of attack, taking Liddament's data database as reference, experimental values of facade-averaged C_p differ by up to 30%; the difference rises to 40% when LES is employed, while it is always higher than 50% for RANS.

It is important to notice that pressure coefficients from Liddament [21] are valid for a low-rise building with a length-to-width ratio of 2:1, which is lower than the one of the Heijmans ONE building (2.7:1). In addition, Heijmans ONE has a gable roof, while coefficients in the database are valid for a flat roof. These considerations might explain the differences with both experimental and LES data.

4. BES simulations

4.1. Building geometry and numerical setup

The BES simulations are performed with the non-commercial open-source tool EnergyPlus [10]. The building geometry is identical to the one adopted for the CFD simulations, which is based on the semi-portable and semi-energy autarkic building Heijmans ONE [29]. This building was also used for the BES reported in Vasaturo et al. [64] and can be classified according to ISSO [89] as lightweight since the thermal mass, equal to 14 kg/m^2, is lower than 20 kg/m^2.

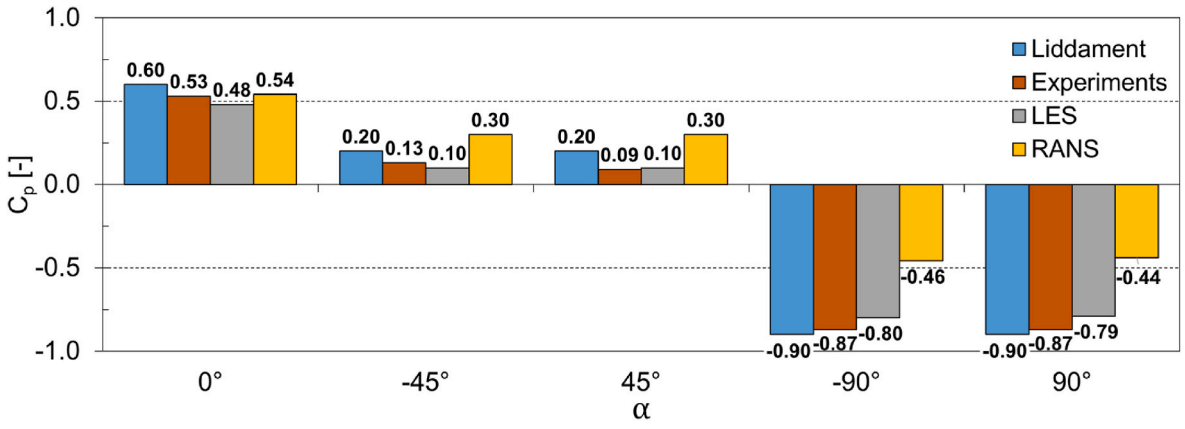

Fig. 11. Facade-averaged C_p employed in BES from different sources. *Front* facade.

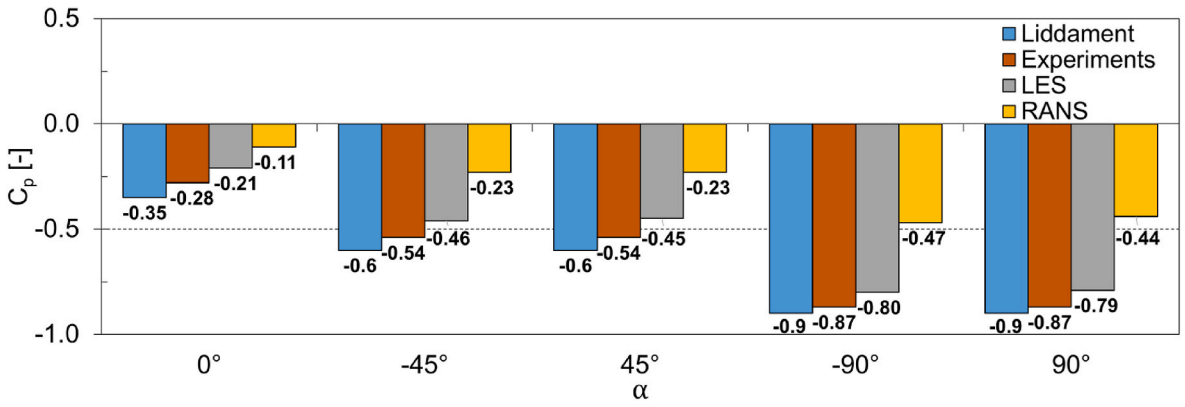

Fig. 12. Facade-averaged C_p employed in BES from different sources. *Back* facade.

Low-emissivity glazing (HR++ [90]) is present on *front* and *back* facades, whereas glazing is absent on lateral facades. In addition, a backdoor is present (Fig. 1). The specific distribution of glazing results in a clear relation between solar heat gain and building orientation, with consequences for the energy consumption of the building [8].

Given the open connection between the two floors of the building, it is modeled in BES as a single zone. The floor is made of different layers, including (outer to inner layer): particleboard panel, polyurethane foam, particleboard panel, PVC panel. The short facades are modeled using timber cladding, air cavity, particleboard panel, polyurethane foam, particleboard panel. For the long facades and the roof, steel cladding is used instead of timber cladding. The building envelope thermal characteristics are reported in Table 4.

Ventilation rate (0.9 dm^3/sm^2, corresponding to 1.1 h^{-1}), temperature setpoints and internal gains (for appliances and occupancy) are the same as adopted by Vasaturo et al. [64] and set according to the Dutch national guidelines [89,91] and building code [92], and in accordance with recommendations by ASHRAE [93]. The algorithms employed to model the convective heat transfer coefficients are those from Montazeri and Blocken [94] for external surfaces and TARP [95] for internal surfaces. The adopted time step is 10 min. An ideal system is assumed for the HVAC system, i.e., in order to meet the heating and cooling loads, a sufficient quantity of conditioned air is supplied to the building [10].

Four climate zones, classified according to Köppen and Geiger [98] are considered for the present work. The simulations are therefore performed for different cities with different climates: Acapulco (Mexico, tropical climate, zone A), Riyadh (Saudi Arabia, dry/desertic climate, zone B), Beek (Netherlands, temperate climate, zone C) and Toronto (Canada, continental climate, zone D). The EPW weather files are downloaded from EnergyPlus.

Eight building orientations (N, NE, E, SE, S, SW, W, NW) are simulated. Natural ventilation is applied as a passive measure to reduce cooling demand, so that the building is cooled by the income of fresh air from the external environment. The effects of natural ventilation are simulated in EnergyPlus using its validated AFN model [10,11]. The windows in Fig. 1 are opened when $T_{zone} > 23°$ and $T_{out} < T_{zone}$, but only from 08:00 to 20:00 h. Pressure coefficients for *front* (Fig. 11) and *back* (Fig. 12) facades are taken from four different sources: Liddament [21], experiments, LES, RANS.

Table 4
Thermal characteristics of the building envelope adopted in the BES simulations.

Thermal resistance (opaque surfaces)	5.0 m^2K/W
Thermal transmittance of glazing	1.2 W/m^2K
Solar heat gain coefficient	0.4
Short-wave reflectivity	0.3 (timber cladding [96]) 0.4 (steel cladding [97])
Long-wave emissivity	0.9

4.2. Results

The BES results for the cross-ventilated building using different pressure coefficient sources are reported in this section. The annual heating and cooling energy demands of the building computed using pressure coefficients from Liddament [21] are taken as base case, since this is the most often employed method in the literature.

Results shown in Table 5 are averaged over all the building orientations considered. For the tropical (A; Acapulco) and dry/desertic (B; Riyadh) climate, where the total energy demand is exclusively or mostly

Table 5
Annual energy demand for the case-study building in different climate zones. Differences (in Δ%) refer to the results obtained using C_p from Liddament [21].

Climate zone [98]	C_p source	heating [Δ%]	cooling [Δ%]	total [Δ%]
A (tropical)	Liddament [21]	no heating needed	(311.4 kWh/m^2)	(311.4 kWh/m^2)
	Experiments		<1%	<1%
	LES			
	RANS			
B (dry/desertic)	Liddament [21]	(4.9 kWh/m^2)	(151.9 kWh/m^2)	(156.8 kWh/m^2)
	Experiments	−2.0%	<1%	<1%
	LES	−4.1%		
	RANS	−4.1%		
C (temperate)	Liddament [21]	(109.4 kWh/m^2)	(6.8 kWh/m^2)	(116.2 kWh/m^2)
	Experiments	−1.4%	<1%	−1.3%
	LES	−2.8%	<1%	−2.7%
	RANS	−3.0%	+1.5%	−2.8%
D (continental)	Liddament [21]	(158.4 kWh/m^2)	(15.6 kWh/m^2)	(174.0 kWh/m^2)
	Experiments	−1.6%	+1.9%	−1.3%
	LES	−2.7%	+2.6%	−2.2%
	RANS	−2.8%	+2.6%	−2.3%

(97%) constituted by the cooling demand (311.4 and 151.9 kWh/m^2 for the base case, respectively) a modest impact (<1%) on the annual cooling (and total) energy demand is observed when different C_p sources are used with respect to the base case. That can be explained by the fact that the outdoor air temperature is larger than the indoor temperature ($T_{out} > T_{zone}$) for most of the day, hence the role of natural ventilation as adaptation measure is marginal with respect to the air conditioning for these two cases. For climate zone C (temperate; Beek), for which the cooling energy demand is very low (6.8 kWh/m^2), the impact of the source of C_p is not quantitively relevant; as a matter of fact, when C_p values from LES and experiments are used, the differences in cooling demand are lower than 1% with respect to the base case, while a slightly higher deviation (+1.5%) is obtained when C_p values from RANS are used. Similarly, for the continental climate (D; Toronto), where the impact of cooling demand is also modest (15.6 kWh/m^2), the difference between the base case and the results obtained using experimental (+1.9%), LES and RANS (+2.6% for both) C_p values is limited. In particular, no differences are observed between RANS and LES cases. In conclusion, from the results obtained so far it is possible to state that, for the present case, the impact of the C_p source on the cooling demand is negligible.

The annual heating energy demand is zero for climate zone A, modest for zone B (4.9 kWh/m^2, about 3% of the total) and more substantial for climate zones C and D (109.4 and 158.4 kWh/m^2 for the base case, respectively) for which it constitutes over 90% of the total demand. For temperate and continental climate, it is therefore important to notice that the impact of the source of C_p values on the heating demand is not negligible for an accurate quantification of the energy consumption. As a matter of fact, using C_p from experiments results in a difference of −1.4% for climate zone C and −1.6% for climate zone D. These differences are higher when CFD is used (about 3%). That can be explained by the fact that the opening model used in EnergyPlus assumes the presence of cracks when windows or doors are closed. In particular, four cracks are generated along the opening. The crack equation [10] used to compute the air mass flow due to the cracks, Q, is

$$Q = KC(\Delta P_c)^n \tag{9}$$

Crack flow is therefore a function of the pressure difference across the crack ΔP_c. The other factors in Eq. (9) are the crack factor, K, the air flow exponent, n, and the product of temperature correction factor times the air mass flow coefficient, C. The pressure coefficients of the facades influence ΔP_c, which therefore influences the crack flow and eventually the heating demand. In order to demonstrate that, two simulations are performed using different C_p sources but removing the effect of cracks; in that case no difference is found in terms of heating demand. Despite the large differences in terms of pressure coefficients, results obtained using RANS and LES as C_p sources are similar for zones B, C and D. This is attributable to the large overestimation of C_p values with RANS technique on both *front* and *back* facades, which causes a net effect (ΔP_c) on the crack flow (Eq. (8)) similar to the LEs case. In addition, a reduced difference is obtained between the case with experimental C_p values and the base case.

Table 6
Peak heating and cooling demands for the case-study building in different climate zones. Differences (in Δ%) refer to the results obtained using C_p from Liddament [21].

Climate zone [98]	C_p source	peak heating [Δ%]	peak cooling [Δ%]
A (tropical)	Liddament [21]	no heating needed	(3.52 kW)
	Experiments		−0.6%
	LES		−1.2%
	RANS		−1.2%
B (dry/desertic)	Liddament [21]	(2.13 kW)	(3.27 kW)
	Experiments	+1.4%	−7.5%
	LES	<1%	−10.2%
	RANS	<1%	−10.8%
C (temperate)	Liddament [21]	(3.65 kW)	(2.14 kW)
	Experiments	<1%	
	LES		
	RANS		
D (continental)	Liddament [21]	(4.67 kW)	(2.45 kW)
	Experiments	−1.8%	
	LES	−1.9%	<1%
	RANS	−1.9%	

The impact of C_p source on peak loads is reported in Table 6. The effect on peak cooling loads is negligible for most of the cases considered, except for climate zone B, for which differences, averaged over all the orientations, by up to 10.8% and, for specific orientations, by up to 20%, are found with respect to the base case. For example, when the building is oriented towards south, using LES and RANS as C_p sources reduces peak loads by 19.1% and 20%, respectively, while a reduction of 15.6% is observed when experimental C_p values are adopted. This is attributable to the effect of heat addition by infiltration, which is higher when pressure coefficients from database are used. Similarly, for climate zone D, for which the peak heating load is the highest among the climate zones considered, variations of peak loads are observed due to a larger amount of heat removed by infiltration when database coefficients are used; nevertheless, differences averaged over all the orientations are lower than 2%, with respect to the base case, when other C_p sources are employed. For specific orientations, e.g., SW, reduction of peak loads differs by up to 3.4% when C_p from RANS and LES are used; similar results (−3.3%) are obtained with experimental pressure coefficients.

The impact of the orientation of the Heijmans ONE building on annual heating and cooling energy demand is reported and discussed in detail in the work of Vasaturo et al. [64]. In general, given the peculiar distribution of glazing on the building (mostly on the *front* facade), the highest value of heating energy demand is found when the building faces north due to a reduced solar heat gain through windows and glass door. For the same reason, the minimum heating demand occurs when the building is oriented towards the south. This is visible, for instance, in the radial plots shown in Fig. 13, where the results of heating demand for the continental climate zone (the case with highest heating demand) are displayed. RANS results are very close to LES and therefore not reported. In agreement with Table 4, the calculated heating demand when experiments (Fig. 13b) and CFD (Fig. 13c) are used as C_p sources is lower. The observed lower values for heating demand are almost homogeneously distributed among the 8 building orientations.

As far as the cooling energy demand is concerned, the tropical climate zone is taken as an example to examine the impact of sources of C_p values for different orientations. An important factor is the latitude and, as consequence, the solar inclination during the year and during the day [8]. The highest value of cooling demand is found when the building orientations are E and W (Fig. 14). That is caused by the larger amount of solar radiation that enters the building with respect to the other directions. In particular, the solar radiation enters though the *front* (E) or *back* (W) facade during the early hours of the day and on the opposite facade in the late afternoon (when the solar inclination is low). For higher latitudes, e.g., for climate zone C, the highest value of cooling demand is found when the building faces SE and SW as already reported in Vasaturo et al. [64]. Similarly, to heating demand, the lower cooling demand obtained when using experiments or CFD is homogeneous for all the building orientations considered.

In conclusion, for both annual heating and cooling it is possible to state that the impact of building orientation is not significantly affected by the adopted C_p source.

5. Discussion, limitations and future work

5.1. Discussion

The results shown in Section 3, where the prediction of pressure coefficients on the Heijmans ONE building is performed by means of full-

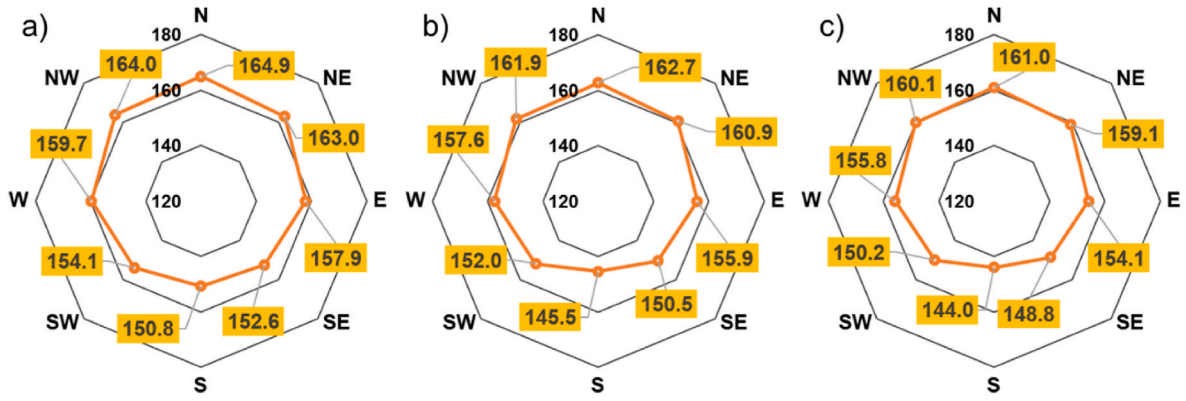

Fig. 13. Effect of the building orientation on the heating demand (in kWh/m^2) for the building in the climate zone D. From left to right, results obtained using as C_p source: (a) Liddament [21]; (b) experiments; c) LES.

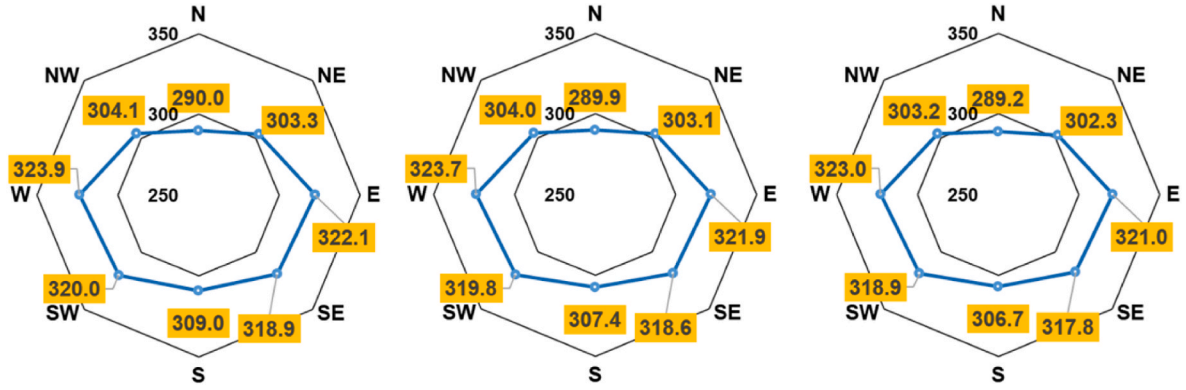

Fig. 14. Effect of the building orientation on the cooling demand (in kWh/m^2) for the building in the climate zone A. From left to right, results obtained using as C_p source: (a) Liddament [21]; (b) experiments; c) LES.

scale CFD simulations, confirm that the prediction of C_p with RANS is satisfactory only for the windward facade and only when the facade itself is perpendicular to the wind direction. For the other facades a large overprediction of C_p is obtained. Employing LES results in a more accurate prediction of pressure coefficients for most locations considered; however, local discrepancies are present, especially in critical flow points like facade corners, where the flow separates and subsequently reattaches to the building. In terms of average values, for all the lateral and leeward facades for all the wind directions considered a closer agreement is found for LES than for RANS. In conclusion, LES outperforms RANS for this kind of prediction, as previously reported in the literature for other building geometries (e.g., Ref. [13,20,48–51]). However, it is important to notice that the grid used for RANS simulations is the same of LES, i.e., a non-conformal grid, which has been successfully used for LES applications (e.g. Ref. [60]), but not for RANS applications, for which the guidelines suggest a limited ratio between two consecutive cells [57,58]. As an example, Montazeri and Blocken [18] showed that an acceptable agreement between experiments and CFD (RANS) is obtained for an isolated, square, medium rise building without balconies not only for the windward facade, but also for the leeward facade, provided that the wind direction is perpendicular to the windward facade. Similarly, Xing and Mohotti [17] obtained a satisfactory agreement in terms of mean pressure coefficients for a gable roof building using RANS. A further limitation of the present study is that LES simulations in this manuscript consider only one subgrid-scale (SGS) model and one inflow turbulence generator. Comparative studies are present in literature regarding the effect of SGS models [19] and inflow generators [99] on the mean pressure distribution on buildings. It should be noted that a previous study by the authors [74] showed that the used inflow generator (vortex method) was the most effective option, combining computational cost and accuracy for a cross-ventilated building. The employed SGS model (KET) resulted the most accurate among those considered in their study.

With respect to the wind-tunnel tests, it is worthwhile mentioning, as a limitation, that the number of pressure taps employed (128) does not allow for a complete characterization of the pressure on the building. As a consequence, pressure field characteristics in critical zones (e.g., detached flow, maximum pressure location) might not have been fully captured.

Table 7
Average values over eight orientations of infiltration rates for different climate zones. Differences (in Δ%) refer to the results obtained using C_p from Liddament [21].

Climate zone [98]	C_p source	Infiltration rate [Δ%]
A (tropical)	Liddament [21]	(0.10 h^{-1})
	Experiments	−7.4%
	LES	−11.8%
	RANS	−12.5%
B (dry/desertic)	Liddament [21]	(0.46 h^{-1})
	Experiments	−7.9%
	LES	−14.1%
	RANS	−14.9%
C (temperate)	Liddament [21]	(0.37 h^{-1})
	Experiments	−7.8%
	LES	−15.2%
	RANS	−16.0%
D (continental)	Liddament [21]	(0.51 h^{-1})
	Experiments	−6.9%
	LES	−13.1%
	RANS	−13.9%

BES results reported in Section 4 demonstrate that the choice of C_p for the present case does not significantly influence the cooling demand when natural ventilation is employed. As a matter of fact, for tropical and dry/desertic climate zones, where most of the energy demand is due to cooling, the impact is lower than 1% with respect to the base case (C_p from database). Nevertheless, for the dry/desertic climate zone, a significant impact of C_p source on peak cooling load is found due to differences in the predicted values of heat addition by infiltration. For colder climates, a slightly higher impact of the C_p source on the annual cooling energy demand is found, which is, however, limited in absolute terms, given the limited cooling demand for those type of climates. Moreover, in Table 7, the impact of the C_p source on infiltration rates, which includes the contribution of natural ventilation, is reported. Although the predicted values might vary, according to the climate zone considered, from −6.9% to −16% with respect to the base case, the impact of the C_p source in absolute terms is limited for the case under examination. For cases with more and/or larger openings the impact of the C_p source on the energy demand could become more pronounced; future studies are recommended on this aspect.

On the other hand, the impact of C_p source on the heating demand is more relevant than the cooling demand due to the presence of cracks; the crack flow is directly influenced by the C_p. As a result, for the climates with higher heating demand (climate zones C and D), a difference of up to 3% is found. Although this discrepancy might appear limited, the uncertainty due to the source of C_p values must be taken into account for a correct assessment of the BES results when the heating demand is computed. For example, in Vasaturo et al. [64] it is shown that – with the same building, climate, and C_p coefficients from Liddament [21] – increasing the thermal resistance of the envelope to 6.5 m^2K/W reduces the heating demand by 8%. In comparison, the impact of source of C_p values on the computed heating energy demand is a bit less than half with respect to a measure to reduce heating demand such as increasing the thermal resistance.

In conclusion, it seems reasonable to state that, for this construction typology (low-rise building with gable roof) and the climate zones considered, the impact of the numerical technique is of paramount importance for the prediction of C_p, but the source of C_p values itself does not significantly influence the results in terms of annual cooling demand. Hence, if the aim of the BES is the prediction of the annual cooling demand, or the annual heating demand is not relevant, C_p from databases could be used as source at first. However, it must be noted that, for dry/desertic climates, the C_p source does impact the estimated peak cooling load. For the accurate prediction of heating demand in cold climates at least the uncertainty due to the adopted C_p source must be taken into account. For complex building geometries, for which no data on pressure coefficients are available, if the principal aim of the CFD simulation is to provide average C_p as input for the subsequent BES simulation, it is recommended to run a less computationally demanding RANS simulation as a first step, rather than LES or performing experiments. Conversely, if the objective of the simulation is the accurate prediction of C_p distributions, LES is recommended, possibly with experiments to validate the numerical results.

5.2. Limitations and future work

Some limitations of the study presented in this paper, a part of which will be addressed in future work, are reported below.

- The impact of the C_p source on other relevant parameters for a residential building (e.g., natural flow rates and overheating) is not addressed in this study.
- The use of more advanced multizone simulations tools, such as CONTAM, in combination with CFD was out of the scope of this paper but is an interesting research direction for future work.
- Surface-averaged C_p coefficients are employed in BES, while choosing local C_p values might have an impact on the results, as discussed by Wang et al. [46] for the CONTAM software. A more detailed analysis of spatial variation of C_p and its effects on BES will be presented as part of future work.
- The use of multizone models for the assessment of cross-ventilation flows has its shortcomings, however, it is also not feasible to run CFD simulations for all cases. Furthermore, the aim of the current study is not to analyze whether the flow rates are accurately predicted in EnergyPlus; in fact, the present work merely assesses the effects of different C_p sources on the predictions of airflow and energy use by a multizone model. Future work could focus on the accuracy of cross-ventilation flow predictions in multizone models and how CFD can be used to improve accuracy.
- A larger influence of the C_p source might be obtained in studies of more complex buildings in urban areas. Further studies are needed in that respect.

6. Conclusions

In the present work the impact of the source of pressure coefficients on the BES results of an isolated lightweight naturally ventilated building is assessed in terms of annual energy demand for heating and cooling. In particular the following conclusions can be made.

- Full-scale CFD results obtained using RANS and LES techniques are compared with experimental results on a reduced-scale (1:40) building. Numerical results from LES agree well with the wind tunnel data in terms of C_p on all locations considered, while RANS largely overpredicts C_p for lateral and leeward facades. The same consideration applies to the average pressure coefficients. Experimental and LES mean C_p of the *front* facade deviate from database coefficients by up to 50% for oblique wind directions, and up to 30% for $\alpha = 0^\circ$. Lower differences are found for the other wind directions. For the *back* facade, the differences are up to 40% for $\alpha = 0^\circ$ and lower for the other wind directions.
- For the considered building typology, as a first step employing C_p data from databases is acceptable for predicting cooling demand by means of BES when natural ventilation is present, and AFN is used. If no data are available, RANS is still the best cost-effective choice to obtain mean C_p, since the difference in terms of estimated cooling demand using C_p from LES is negligible.
- The effect of C_p source is more significant for cold climates, where the annual heating demand is prevailing, since the crack flows depend on the pressure difference between the external and internal zones. If data from a database are employed, a possible uncertainty must be taken into account in the annual heating demand calculation, which is quantified to be 3% for the present building.
- The effects of C_p source on peak cooling loads are relevant for dry/desertic climate (up to 10.8%) and, to a lesser extent, on peak heating loads for continental climate (up to 1.9%).

CRediT authorship contribution statement

R. Vasaturo: Writing – original draft, Visualization, Validation, Software, Methodology, Investigation, Formal analysis, Data curation, Conceptualization. **T. van Hooff:** Writing – review & editing, Supervision, Methodology, Conceptualization. **S. Gillmeier:** Writing – review & editing, Investigation, Data curation. **B. Blocken:** Writing – review & editing, Supervision, Methodology, Conceptualization. **P.J.V. van Wesemael:** Writing – review & editing, Supervision.

Declaration of competing interest

The authors declare the following financial interests/personal relationships which may be considered as potential competing interests: Raffaele Vasaturo reports financial support was provided by Heijmans B. V. Raffaele Vasaturo reports financial support was provided by

Nederlandse Organisatie voor Wetenschappelijk Onderzoek. Bert Blocken (co-author) is currently an editor of Building and Environment.

Data availability

Data will be made available on request.

Acknowledgements

This research was financially supported by the PhD Impulse Program of the Eindhoven University of Technology, in collaboration with the construction company Heijmans B.V., the Netherlands. This work has been sponsored by NWO *Exacte en Natuurwetenschappen* (Physical Sciences) for the use of supercomputer facilities, with financial support from the *Nederlandse Organisatie voor Wetenschappelijk Onderzoek* (Netherlands Organization for Scientific Research, NWO). The authors gratefully acknowledge the partnership with ANSYS CFD.

References

[1] M. Santamouris, D. Kolokotsa, Passive cooling dissipation techniques for buildings and other structures, Energy Build. 57 (2013) 74–94.
[2] A. Pino, W. Bustamante, R. Escobar, F. Encinas, F.E. Pino, Thermal and lighting behavior of office buildings in Santiago of Chile, Energy Build. 47 (2012) 441–449.
[3] R. Ramponi, A. Angelotti, B. Blocken, Energy saving potential of night ventilation: sensitivity to pressure coefficients for different European climates, Appl. Energy 123 (2014) 185–195.
[4] H. Wang, Q. Chen, Impact of climate change heating and cooling energy use in buildings in the United States, Energy Build. 82 (2014) 428–436.
[5] T. van Hooff, B. Blocken, J.L.M. Hensen, H.J.P. Timmermans, On the predicted effectiveness of climate adaptation measures for residential buildings, Build. Environ. 82 (2014) 300–316.
[6] T. van Hooff, B. Blocken, H.J.P. Timmermans, J.L.M. Hensen, Analysis of the predicted effect of passive climate adaptation measures on energy demand for cooling and heating in a residential building, Energy 94 (2016) 811–820.
[7] L. Pierangioli, G. Cellai, R. Ferrise, G. Trombi, M. Bindi, Effectiveness of passive measures against climate change: case studies in Central Italy, Build. Simulat. 10 (2017) 459–479.
[8] R. Vasaturo, T. van Hooff, I. Kalkman, B. Blocken, P. van Wesemael, Impact of passive climate adaptation measures and building orientation on the energy demand of a detached lightweight semi-portable building, Build. Simulat. 11 (2018) 1163–1177.
[9] J. Cheng, D. Qi, A. Katal, L. Wang, T. Stathopoulos, Evaluating wind-driven natural ventilation potential for early building design, J. Wind Eng. Ind. Aerod. 182 (2018) 160–169.
[10] EnergyPlus, EnergyPlus Documentation - Engineering Reference: the Reference to EnergyPlus Calculations, 2010.
[11] Z. Zhai, M.H. Johnson, M. Krarti, Assessment of natural and hybrid ventilation models in whole-building energy simulations, Energy Build. 43 (2011) 2251–2261.
[12] G.N. Walton, *AIRNET – A Computer Program For Building Airflow Network Modeling*. NISTIR 89-4072, 1989 (Washington, DC, USA).
[13] D. Cóstola, B. Blocken, J.L.M. Hensen, Overview of pressure coefficient data in building energy simulation and airflow network programs, Build. Environ. 44 (2009) 2027–2036.
[14] G.M. Richardson, D. Surry, Comparisons of wind-tunnel and full-scale surface pressure measurement on low-rise pitched-roof buildings, J. Wind Eng. Ind. Aerod. 38 (1991) 249–256.
[15] H. Okada, Y.C. Ha, Comparison of wind tunnel and full-scale pressure measurement tests in the Texas Tech Building, J. Wind Eng. Ind. Aerod. 1992 (1992) 1601–1612.
[16] P.J. Richards, R.P. Hoxey, B.D. Connell, D.P. Lander, Wind-tunnel Modelling of the Silsoe Cube, 2007.
[17] F. Xing, D. Mohotti, Experimental and numerical study on mean pressure distributions around an isolated gable roof building with and without openings, Build. Environ. 132 (2018) 30–44.
[18] H. Montazeri, B. Blocken, CFD simulation of wind-induced pressure coefficients on buildings with and without balconies: validation and sensitivity analysis, Build. Environ. 60 (2013) 137–149.
[19] R.H. Ong, L. Patruno, D. Yeo, Y. He, K.C.S. Kwok, Numerical simulation of wind-induced mean and peak pressures around a low-rise structure, Eng. Struct. 214 (2020) 110583.
[20] X. Zheng, H. Montazeri, B. Blocken, CFD simulations of wind flow and mean surface pressure for buildings with balconies: comparison of RANS and LES, Build. Environ. 173 (2020) 106747.
[21] M.W. Liddament, AIVC: a Guide to Energy Efficient Ventilation, AIVC, Coventry, UK, 1996.
[22] American Society of Heating Refrigerating and Air-Conditioning Engineers (ASHRAE), International Weather for Energy Calculations (IWEC Weather Files), 2001.
[23] M. Grosso, Wind pressure distribution around buildings: a parametrical mode, Energy Build. 18 (1992) 101–131.
[24] B. Knoll, J.C. Phaff, W.F. de Gids, Pressure simulation program, in: Proceedings of the 16th AIVC Conference – Implementing the Results of Ventilation Research, Palm Springs, USA, 1995. September 19-22.
[25] Eurocode, Eurocode 1: actions on structures – Part 1-4: general actions – wind actions, Eur. Comm. Stand. 4 (2005) 1–148.
[26] Air Infiltration and Ventilation Centre (AIVC), Wind Pressure Workshop Proceedings AIC-TN-13, 1984, pp. 1–84 (Brussels, Belgium).
[27] S. de Wit, G. Augenbroe, Uncertainty analysis of building design evaluations, in: Proceedings of Building Simulation 2001: 7th Conference of IBPSA. August 13-15, Rio de Janeiro, Brazil, 2001.
[28] S. de Wit, *Uncertainty In Predictions of Thermal Comfort in Buildings* (PhD Thesis), Delft University of Technology, 2001.
[29] B.V. Heijmans, Heijmans ONE. Prijsoverzicht en Technische Beschriving, 2016. Available at: https://www.heijmans.nl/media/filer_public/1d/a5/1da5cb9c-319d-4b92-8629-5fb6ae254ba0/bijlage_prijs-technisch_heijmans_one.pdf.
[30] W. Tian, X. Han, W. Zuo, M.D. Sohn, Building energy simulation coupled with CFD for indoor environment: a critical review and recent applications, Energy Build. 165 (2018) 184–199.
[31] N. Lauzet, A. Rodler, M. Musy, M.H. Azam, S. Guernouti, D. Mauree, T. Colinart, How building energy models take the local climate into account in an urban context – a review, Renew. Sustain. Energy Rev. (2019) 109390.
[32] M. Rodríguez-Vázquez, I. Hernández-Pérez, J. Xamán, Y. Chávez, M. Gijón-Rivera, J.M. Belman-Flores, Coupling building energy simulation and computational fluid dynamics: an overview, J. Build. Phys. 44 (2) (2020) 137–180.
[33] N. Sezer, H. Yoonus, D. Zhan, L. Wang, I.G. Hassan, M.A. Rahman, Urban microclimate and building energy models: a review of the latest progress in coupling strategies, Renew. Sustain. Energy Rev. (2023) 113577.
[34] Q. Chen, Z. Zhai, L. Wang, Computer modeling of multiscale fluid flow and heat and mass transfer in engineered spaces, Chem. Eng. Sci. 62 (2007) 3580–3588.
[35] I. Beausoleil-Morrison, The adaptive conflation of computational fluid dynamics with whole-building thermal simulation, Energy Build. 34 (2002) 857–871.
[36] Z. Zhai, Q. Chen, P. Haves, J.H. Klems, On approaches to couple energy simulation and computational fluid dynamics program, Build. Environ. 37 (2002) 857–864.
[37] Z. Zhai, Q. Chen, Solution characters of iterative coupling between energy simulation and CFD programs, Energy Build. 35 (2003) 493–505.
[38] A. Mochida, H. Yoshino, S. Miyauchi, T. Mitamura, Total analysis of cooling effects of cross-ventilation affected by microclimate around a building, Sol. Energy 80 (2006) 371–382.
[39] Y. Pan, Y. Li, Z. Huang, G. Wu, Study on simulation methods of atrium building cooling load in hot and humid regions, Energy Build. 42 (2010) 1654–1660.
[40] M. Barbason, S. Reiter, Coupling building energy simulation and computational fluid dynamics: application to a two-storey house in a temperate climate, Build. Environ. 75 (2014) 30–39.
[41] R. Zhang, P.A. Mirzaei, B. Jones, Development of a dynamic external CFD and BES coupling framework for application of urban neighbourhoods energy modelling, Build. Environ. 146 (2018) 37–49.
[42] O.S. Asfour, M.B. Gadia, A comparison between CFD and Network models for prediction wind-driven ventilation in buildings, Build. Environ. 42 (2007) 4079–4085.
[43] Z. Zhai, Q. Chen, Performance of coupled building energy and CFD simulations, Energy Build. 37 (2005) 333–344.
[44] D. Cóstola, M. Alucci, Pressure coefficient simulated by CFD for wind-driven ventilation analysis, in: Proceedings of Building Simulation 2007: 10th Conference of IBPSA, 2007, pp. 999–1006. July 27-30. Beijing, China.
[45] L. Wang, N.H. Wong, Coupled simulations for naturally ventilated residential buildings, Autom. ConStruct. 17 (4) (2008) 386–398.
[46] L. Wang, W.S. Dols, Q. Chen, Using CFD capabilities of CONTAM 3.0 for simulating airflow and contaminant transport in and around buildings, HVAC R Res. 6 (3) (2010) 749–763.
[47] S. Charisi, N. Waszczuk, T.K. Thiis, Determining building-specific wind pressure coefficients to account for the microclimate in the calculation of air infiltration in buildings, Adv. Build. Energy Res. 15 (3) (2021) 368–389.
[48] Y. Jiang, Q. Chen, Study of natural ventilation in buildings by large eddy simulation, J. Wind Eng. Ind. Aerod. 89 (2001) 1155–1178.
[49] T. Yang, N.G. Wright, D. Etheridge, A. Quinn, A comparison of CFD and full-scale measurements for analysis of natural ventilation, Int. J. Vent. 4 (2006) 337–348.
[50] T. Nozu, T. Tamura, Y. Okuda, S. Sanada, LES of the flow and building wall pressures in the center of Tokyo, J. Wind Eng. Ind. Aerod. 96 (2008) 1762–1773.
[51] Y. Tominaga, A. Mochida, S. Murakami, S. Sawaki, Comparison of various revised k-ε models and LES applied to flow around a high-rise building model with 1:1:2 shape placed within the surface boundary layer, J. Wind Eng. Ind. Aerod. 96 (2008) 389–411.
[52] B. Blocken, LES over RANS in building simulation for outdoor and indoor applications: a foregone conclusion? Build. Simulat. 11 (5) (2018) 821–870.
[53] B.V. Heijmans, Heijmans ONE, 2018. Available at: https://www.heijmans.nl/nl/heijmans-one.
[54] B. Blocken, T. Stathopoulos, J. Carmeliet, Wind environmental conditions in passages between two long narrow perpendicular buildings, J. Aero. Eng. 21 (4) (2008) 280–287.
[55] VDI 3783-12, Environmental meteorology: physical modelling of flow and dispersion processes in the atmospheric boundary layer - application of wind tunnels, in: Verein Deutscher Ingenieure, Kommision Reinhaltung der Luft (KRdL) im VDI und DIN - Normenausschuss, Beuth Verlag, Berlin, Germany, 2000.

[56] Y. Tominaga, B. Blocken, Wind tunnel experiments on cross-ventilation flow of a generic building with contaminant dispersion in unsheltered and sheltered conditions, Build. Environ. 92 (2015) 452–461.
[57] Y. Tominaga, A. Mochida, R. Yoshie, H. Kataoka, T. Nozu, M. Yoshikawa, T. Shirasawa, AIJ guidelines for practical applications of CFD to pedestrian wind environment around buildings, J. Wind Eng. Ind. Aerod. 96 (2008) 1749–1761.
[58] J. Franke, A. Hellsten, H. Schlünzen, B. Carissimo, Best practice guideline for the CFD simulation of flows in the urban environment, Cost Action 732 (2007).
[59] B. Blocken, Computational Fluid Dynamics for urban physics: importance, scales, possibilities, limitations and ten tips and tricks towards accurate and reliable simulations, Build. Environ. 91 (2015) 219–245.
[60] S. Iousef, H. Montazeri, B. Blocken, P.J.V. van Wesemael, On the use of non-conformal grids for economic LES of wind flow and convective heat transfer for a wall-mounted cube, Build. Environ. 119 (2017) 44–61.
[61] ANSYS Fluent, Release 15.0, Theory Guide, ANSYS Inc, November 2013.
[62] Snyder, Similarity criteria for the application of fluid models to the study of air pollution meteorology, Bound.-layer Meteorol. 3 (1972) 113–134.
[63] P.Y. Cui, W.Q. Chen, J.Q. Wang, J.H. Zhang, Y.D. Huang, W.Q. Tao, Numerical studies on issues of Re-independence for indoor airflow and pollutant dispersion within an isolated building, Build. Simulat. 15 (2022) 1259–1276.
[64] R. Vasaturo, I. Kalkman, B. Blocken, P.J.V. van Wesemael, Large eddy simulation of the neutral atmospheric boundary layer: performance evaluation of three inflow methods for terrains with different roughness, J. Wind Eng. Ind. Aerod. 173 (2018) 241–261.
[65] F. Mathey, D. Cokliat, P. Bertoglio, E. Sergent, Specification of LES inlet boundary condition using vortex method, in: 4th International Symposium on Turbulence, Heat and Mass Transfer, 2003 (Antalya, Turkey).
[66] F. Mathey, D. Cokliat, P. Bergoglio, E. Sergent, Assessment of the vortex method for large eddy simulation inlet conditions, Prog. Comput. Fluid Dynam. Int. J. 6 (2006) 58–67.
[67] E. Sergent, *Vers une méthodologie de couplage entre la simulation des grandes echelles et les modèles statistiques* (PhD thesis), École Centrale de Lyon, 2002.
[68] P. Gousseau, B. Blocken, T. Stathopoulos, G.J.F. van Heijst, CFD simulation of a near-field pollutant dispersion on a high-resolution grid: a case study by LES and RANS for a building group in downtown Montreal, Atmos. Environ. 45 (2) (2011) 428–438.
[69] P. Gousseau, B. Blocken, G.J.F. van Heijst, CFD simulation of pollutant dispersion around isolated buildings: on the role of convective and turbulent mass fluxes in the prediction accuracy, J. Hazard Mater. 194 (2011) 422–434.
[70] P. Gousseau, B. Blocken, G.J.F. van Heijst, Quality assessment of Large-Eddy Simulation of wind flow around a high-rise building: validation and solution verification, Comput. Fluids 79 (2013) 120–133.
[71] P. Gousseau, B. Blocken, T. Stathopoulos, G.J.F. van Heijst, Near-field pollutant dispersion in an actual urban area: analysis of the mass transport mechanism by high-resolution Large Eddy Simulation, Comput. Fluids 114 (2015) 151–162.
[72] T. van Hooff, B. Blocken, P. Gousseau, G.J.F. van Heijst, Counter-gradient diffusion in a slot-ventilated enclosure assessed by LES and RANS, Comput. Fluids 94 (2014) 63–75.
[73] T. van Hooff, B. Blocken, Y. Tominaga, On the accuracy of CFD simulations of cross-ventilation flows for a generic isolated building: comparison of RANS, LES and experiments, Build. Environ. 114 (2017) 148–165.
[74] R. Vasaturo, Numerical Simulation of the Atmospheric Boundary Layer with Application to Natural Ventilation, Eindhoven University of Technology, 2023 (Chapter 3). PhD thesis.
[75] P.J. Richards, R.P. Hoxey, Appropriate boundary conditions for computational wind engineering models using the k-ε turbulence model, J. Wind Eng. Ind. Aerod. 46–47 (1993) 145–153.
[76] S. Iousef, H. Montazeri, B. Blocken, P.J.V. van Wesemael, Wall-resolved versus wall-modeled LES of the flow field and surface forced convective heat transfer for a low-rise building, Build. Environ. 244 (2023) 110678.
[77] X. Zheng, H. Montazeri, B. Blocken, Impact of building façade geometrical details on pollutant dispersion in street canyons, Build. Environ. 212 (2022) 108746.
[78] J. Kim, P. Moin, Application of a fractional-step method to incompressible Navier-Stokes equations, J. Comput. Phys. 59 (1985) 308–323.
[79] J.B. Bell, P. Colella, H.M. Glaz, A second-order projection method for the incompressible Navier-Stokes equations, J. Comput. Phys. 85 (1989) 257–283.
[80] J.K. Dukowicz, A.S. Dvinsky, Approximate factorization as a high order splitting for the implicit incompressible flow equations, J. Comput. Phys. 102 (1992) 336–347.
[81] J. Perot, An analysis of the fractional step method, J. Comput. Phys. 108 (1993) 51–58, 1993.
[82] S. Armfield, R. Street, The fractional-step method for the Navier-Stokes equations on staggered grids: the accuracy of three variations, J. Comput. Phys. 153 (1999) 660–665.
[83] W.W. Kim, S. Menon, Technical Report AIAA-97-0210, American Institute of Aeronautics and Astronautics, 35th Aerospace Sciences Meeting, Reno, USA, 1997.
[84] T.H. Shih, W.W. Liou, A. Shabbir, Z. Yang, J. Zhu, A new k-epsilon eddy viscosity model for high Reynolds number turbulent flows, Comput. Fluids 24 (1995) 227–238.
[85] I. Celik, Z.N. Cehreli, I. Yavuz, Index of resolution qualify for large eddy simulation, J. Fluid Eng. 127 (2005) 949–958.
[86] S.B. Pope, Turbulent Flows, Cambridge University Press, 2000.
[87] M. Schatzmann, H. Olesen, J. Franke, COST 732 Model Evaluation Case Studies: Approach and Results, 2010 (Cost Action).
[88] S. Murakami, Comparison of various turbulence models applied to a bluff body, J. Wind Eng. Ind. Aerod. 46–47 (1993) 21–36.
[89] ISSO, Publicatie 32: Uitgangspunten Temperatuursimulatieberekeningen, Stichting ISSO, Rotterdam, The Netherlands, 2011 (in Dutch).
[90] B.V. Kiwa Nederland, Nationale Beoordelingsrichtlijn BRL 2202, Rijswijk, The Netherlands, 2012 (in Dutch).
[91] Ministerie van VROM, Energiegedrag in De Woning, 2009 (in Dutch).
[92] Bouwbesluit online (in Dutch), http://www.bouwbesluitonline.nl, 2012.
[93] American Society of Heating Refrigerating and Air-Conditioning Engineers (ASHRAE), ASHRAE Handbook - HVAC Applications, 2009 (Atlanta, GA, USA).
[94] H. Montazeri, B. Blocken, New generalized expressions for forced convective heat transfer coefficients at building facades and roofs, Build. Environ. 119 (2017) 153–168.
[95] G.N. Walton, Thermal Analysis Research Program Reference Manual, NBSSIR, Washington, DC, USA, 1983, pp. 83–2655.
[96] S. Bretz, H. Akbari, A. Rosenfeld, H. Taha, Implementation of Solar-Reflective Surfaces: Materials and Utility Programs, 1992 (Berkeley, USA).
[97] G. Chin, A. Desjarlais, M. Estes, D. Hitchcock, M. Lewis, D. Parker, J. Rosenthal, L. Ross, S. Ryan, R. Schmeltz, P. Turnbull, B. Zalph, Reducing urban heat islands: compendium of strategies. Cool Roofs, U.S. Environmental Protection Agency, 2014.
[98] W. Köppen, R. Geiger, Klima der Erde, 1954 (in German). Wall Map 1:16 Mill. Klett-Perthes. Gotha, Germany.
[99] B.W. Yan, Q.S. Li, Inflow turbulence generation methods with large eddy simulation for wind effects on tall buildings, Comput. Fluids 116 (2015) 158–175.